Journal of the Meteorological Society of Japan, Vol. 87, No. 1, pp. 171–188, 2009.
DOI:10.2151/jmsj.87.171

Potential Predictability of Tropical Low-level Circulation in CWB GFS Ensemble Hindcast

Jau-Ming CHEN

Institute of Navigation Science and Technology, National Kaohsiung Marine University, Kaohsiung, Taiwan

Research and Development Center, Central Weather Bureau, Taipei, Taiwan

Bin WANG

Department of Meteorology and International Pacific Research Center, University of Hawaii, Hawaii, USA

Jyh-Wen HWU and Ching-Feng SHIH

Research and Development Center, Central Weather Bureau, Taipei, Taiwan

(Manuscript received 31 March 2008, in final form 14 November 2008)

Abstract

This study investigates the major sources of potential predictability and associated regulating processes for summer (JJA) low-level tropical circulations using a 1979–2003 ensemble hindcast made by the Central Weather Bureau (CWB) Global Forecast System (GFS) model. This hindcast is conducted with a two-tier system using the external SST forcing so that it lacks the processes of air-sea interactions. This study focuses on three tropical regions: the eastern Pacific Niño (EPN; 160°E–80°W, 30°S–30°N), the western Pacific monsoon (WPM; 100°E–160°E, 30°S–30°N), and the Indian Ocean monsoon (IOM; 40°E–100°E, 30°S–30°N).

The WPM and IOM circulations are found to have different predictability sources and should be examined separately. The predictability source for the former is primarily from SST anomalies in the tropical eastern Pacific, while SST anomalies in the tropical central Indian Ocean (IO) for the latter. Strong SST anomalies tend to induce persistent and large-amplitude circulation anomalies and by so doing enhance potential predictability. Circulation predictability is generally higher over the WPM and EPN regions than over the IOM region.

cedented 1997–98 El Niño event (Wang et al. 2004). A climate prediction performed with the AGCM using the prescribed (observed or predicted) SST forcing is referred to as the two-tier prediction (Bengtsson et al. 1993). In this prediction, the AGCM rainfall anomalies were produced as a result of the AGCM's passive response to the prescribed SST forcing. However, in reality SST anomalies in the Indian Ocean (IO) and the adjacent western Pacific result in part from atmospheric forcing or evolve as a strongly coupled ocean-atmosphere process (e.g., Wang et al. 2004; Kang and Shukla 2006). Neglect of local monsoon-warm ocean interaction produces an erroneous local SST-rainfall relationship in the two-tier AGCM prediction (Wang et al. 2005). Prediction of summer monsoon rainfall requires investigators to take into account the local air-sea interactions (Wang et al. 2003; Wang et al. 2004; Wu and Kirtman 2005; Kumar et al. 2005). One may expect the coupled ocean-atmosphere model to have better climate prediction skills. However, the climatology of such a coupled model, so far, still has large systematic biases by which its prediction skill is deteriorated (e.g., Kang and Shukla 2006).

In an attempt to improve rainfall prediction in the two-tier system, we turn to examination of the predictability of large-scale circulation anomalies. This was motivated by a previous work by Chen et al. (2005). They have demonstrated that summer rainfall variability in Taiwan and Southeast Asia is markedly influenced by the low-level (850 mb) circulation anomalies associated with the western North Pacific summer monsoon and the Pacific abrupt climate change during the late 1970s. The former affects Taiwan's summer rainfall via regulating vertical motion, while the latter via modulating low-level flows and associated moisture transport. The low-level circulation anomaly is a potentially useful field for predicting summer rainfall over East and Southeast Asia. The performance of climate prediction in these regions should be strongly affected by the predictability of model low-level circulations.

Conventional weather predictability focuses on the accuracy level of weather prediction. For climate predictability, it points to the potentially predictable components or the reproducibility of climate anomalies (e.g., Chen and Van den Dool 1997; Shukla et al. 2000; Kusunoki et al. 2001). In the AGCM ensemble prediction, the potentially predictable component is mainly caused by external SST forcing, while the unpredictable component results from model internal dynamic processes (e.g., Kumar et al. 1996; Rowell 1998; Kumar et al. 2001). Atmospheric climate predictability is inherently limited by the existence of unpredictable internal variability. Potential predictability of model atmospheric anomalies was found to have clear seasonality and regionality. Temporally, it is generally high in winter, but low in summer (e.g., Rowell 1998; Kusunoki and Kobayashi 2003; Zheng et al. 2004). Spatially, it is commonly high in the tropics due to strong air-sea coupling, but low in the extratropics due to vigorous atmospheric high frequency variability (e.g., Sugi et al. 1997; Rowell 1998; Nakaegawa et al. 2003; Kang et al. 2004).

Examination of model potential predictability in the tropics often focuses on the eastern-Pacific El Niño region. The western Pacific and the Indian monsoon regions are normally combined together to be discussed as the predictability of the Asian-Australian (AA) monsoon system (e.g., Sperber et al. 2000; Kang et al. 2004; Wang et al. 2004). Lau et al. (2000) pointed out that the AA monsoon should be separated into the Indian monsoon and the East Asian-western Pacific monsoon owing to different characteristics in their dynamic and boundary forcing. Such differences in monsoon characteristics suggest that the western Pacific monsoon (WPM) and the Indian monsoon may also differ in their predictive characteristics and thus deserve a separate evaluation.

The main purpose of this study is to examine potential predictability of the summer (June–August) tropical low-level circulation from ensemble hindcasts conducted with the Central Weather Bureau (CWB) AGCM (namely, Global Forecast System, GFS) using observed SST forcing. The focus regions include the eastern Pacific, the western Pacific, and the Indian monsoon regions. Low-level circulation is analyzed because it is a large-scale field closely connected to monsoon rainfall over East Asia.

The major issues to be investigated are as follows:

- What are the major predictability features of the tropical circulations in the GFS hindcasts?
- Does potential predictability over the western Pacific connect with that over the Indian monsoon region and the eastern Pacific? If yes, what are the major dynamic processes that give rise to their connection?

- How does the external SST anomaly (SSTA) provide sources of predictability for these tropical circulations in the GFS hindcasts? What are the associated regulating processes?

Results of this study should help us better understand the predictive characteristics of model tropical circulation in two-tier prediction, as well as better maneuver the AGCM's monsoon rainfall prediction for the Asian-western Pacific regions.

2. Model and experimental designs

The CWB GFS is a global spectral primitive equation model with a T42 truncation and 18 vertical levels. Surface fluxes are calculated with Louis (1979) formulas. The vertical turbulence mixing is parameterized by the eddy mixing flux scheme developed by Detering and Etling (1985). Radiative transfer is calculated following the parameterization scheme proposed by Harshvardhan et al. (1987). Cumulus convection is parameterized by a relaxed form of the Arakawa-Schubert convection scheme (Arakawa and Schubert 1974; Moothi and Suarez 1992). The parameterization schemes for shallow convection and gravity wave drag are developed from Tiedtke (1984) and Palmer et al. (1986), respectively. Readers are referred to Liou et al. (1997) for more details of the dynamic and physical schemes used in the GFS.

A 10-member ensemble hindcast is conducted with the GFS using an experimental design similar to that of the Seasonal-prediction Model Intercomparison Project (SMIP; Kusunoki et al. 2001). For the period of 1979–2003, 10 ensemble integrations were carried out for a length of seven months in each year, using initial conditions at 12 UTC from 21 April to 30 April of each year. The initial data used are derived from the National Centers for Environmental Prediction/Department of Energy reanalysis-2 data (Kanamitsu et al. 2002) and the boundary conditions are the observed SSTs from the extended reconstructed SST (ERSST) data compiled by Smith and Reynolds (2003; 2004).

3. Assessment methods

The potential predictability of the model circulation is assessed by two methods. The potentially predictable component of the climate prediction is measured by the signal-to-noise ratio, while the degree of reproducibility is evaluated in terms of the perfect-model pattern correlation. These two methods are briefly described in the following.

3.1 Signal-to-noise ratio

Climate variability in the AGCM experiment may arise from two sources: the unpredictable climate noise resulting from atmospheric internal nonlinear dynamics and the predictable climate signal induced by external SST forcing. The model's potential predictability increases when the predictable signal dominates over the unpredictable noise. This predictability can be measured by the ratio between climate signal and climate noise of the seasonal prediction, namely, the signal-to-noise ratio (Rowell 1998; Shukla et al. 2000). In this measurement, the total variance of the ensemble hindcast (σ^2_{EN}) is divided into two components associated with the climate signal (σ^2_{SIGNAL}) and climate noise (σ^2_{NOISE}). In an n-member hindcast with N years of integration, variance of climate noise can be expressed as:

$$\sigma^2_{NOISE} = \frac{1}{N(n-1)} \sum_{i=1}^{N} \sum_{j=1}^{n} (A_{ij} - \bar{A}_i)^2,$$

where A_{ij} is the predicted field for the ith year of the jth member, and the ensemble mean of the ith year is equal to $\bar{A}_i = \frac{1}{n}\sum_{j=1}^{n} A_{ij}$. Variance of climate signal is obtained by the mean square of the deviation of each year's ensemble mean from the climatological mean ($\bar{\bar{A}} = \frac{1}{N(n)}\sum_{i=1}^{N}\sum_{j=1}^{n} A_{ij}$) and with a consideration for bias correction, as in Rowell (1998):

$$\sigma^2_{SIGNAL} = \sigma^2_{EN} - \frac{1}{n}\sigma^2_{NOISE}, \quad \text{and}$$

$$\sigma^2_{EN} = \frac{1}{N-1} \sum_{i=1}^{N} (\bar{A}_i - \bar{\bar{A}})^2.$$

The potentially predictable region is defined as the area with a signal-to-noise ratio ($\sigma^2_{SIGNAL}/\sigma^2_{NOISE}$) larger than 1 where climate signal dominates over climate noise.

3.2 Perfect-model pattern correlation

The use of perfect boundary condition (i.e., observed SSTs) makes the present hindcast as a perfect-model prediction (e.g., Tribbia and Baumhefner 1988; Zwiers 1996). Its potential predictability can be measured by the perfect-model pattern correlation (PPC), which surveys the reproducibility of climate anomaly in the ensemble hindcast in terms of the degree of pattern resemblance for the selected field between two different members (e.g., Miyakoda et al. 1972; Saha and Van den Dool 1988; Chen and Van den Dool 1997; Shukla et al.

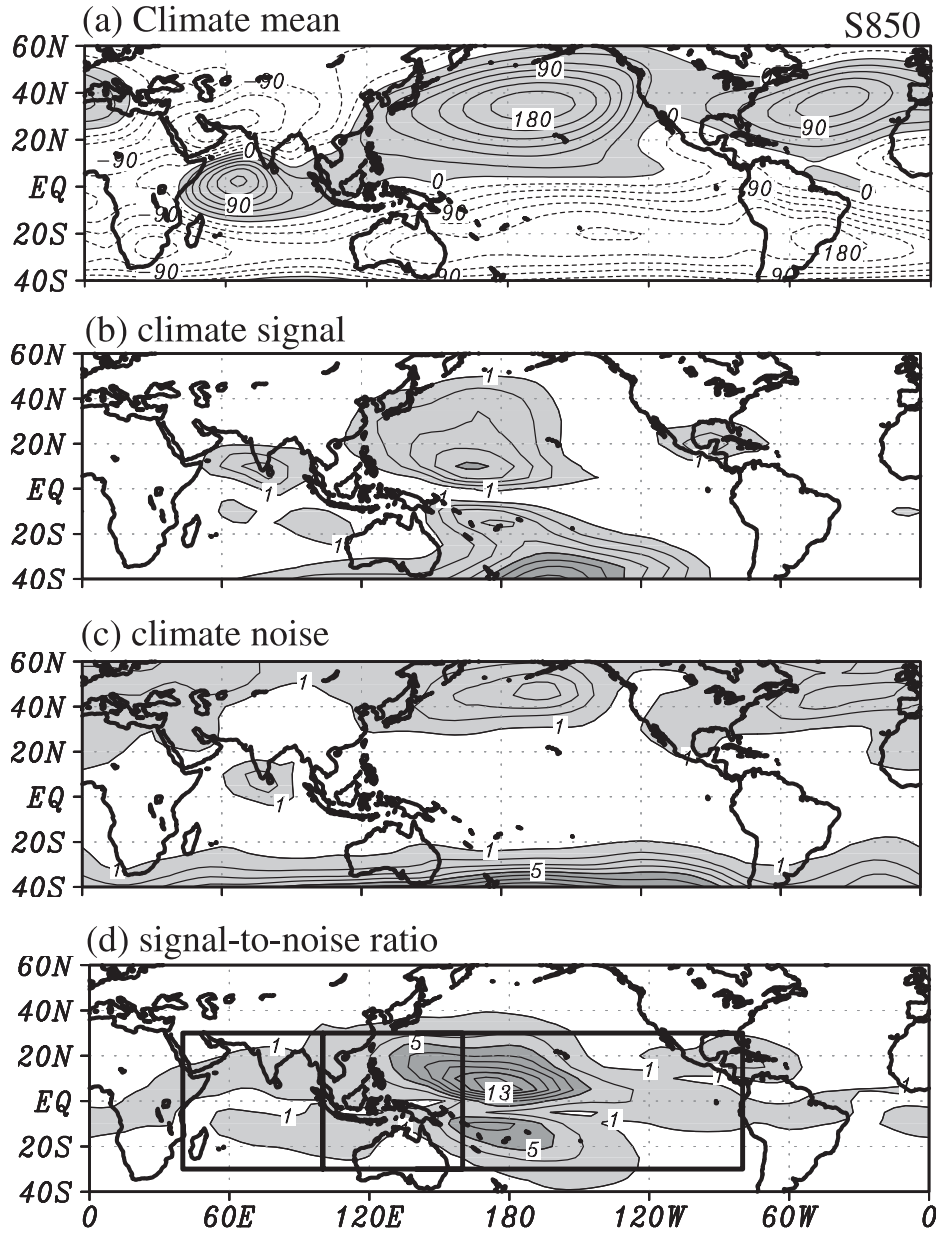

Fig. 1. The (a) climatology, (b) climate signal, (c) climate noise, and (d) signal-to-noise ratio of the 1979–2003 summer 850-mb streamfunction (S850) obtained from the GFS ensemble hindcast. In (a), the contour intervals are 30×10^5 m^2 s^{-1} and positive values are shaded. In (b)–(d), the contour intervals are 2. The heavily shaded regions have the value larger than 5 and lightly shaded regions have the value between 1 and 5 units.

2000). In the 10-member ensemble experiment, there are 45 $\left(C_2^{10} = \frac{10!}{8!2!}\right)$ PPC values in each summer. The PPC value is computed as follows: $\mathrm{PPC} = \frac{[a_{ia}a_{ib}]}{[a_{ia}^2]^{1/2}[a_{ib}^2]^{1/2}}$, where a_{ij} is the anomaly for the ith year of the jth member with respect to the model climatological mean, i.e., $a_{ij} = A_{ij} - \bar{A}$, and the square brackets denote the spatial average of the computed quantity in the selected spatial domain. A high PPC signifies a small spread in the ensemble

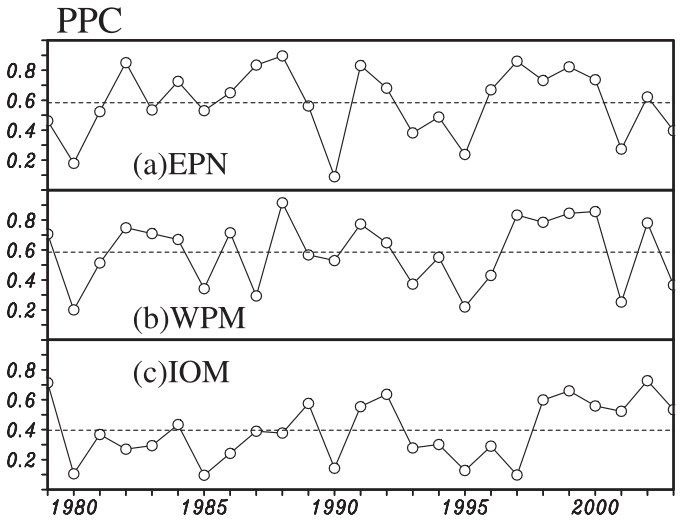

Fig. 2. The 1979–2003 perfect-model pattern correlation (PPC) time series for the GFS summer circulations over three tropical regions: (a) the eastern Pacific Niño (EPN) region (160°E–80°W, 30°S–30°N), (b) the western Pacific monsoon (WPM) region (100°E–160°E, 30°S–30°N), and (c) the Indian Ocean monsoon (IOM) region (40°E–100°E, 30°S–30°N). The horizontal dashed line represents the long-term mean.

prediction and a weak atmospheric internal dynamic or climate noise. The AGCM prediction is dominated by the SST-forced climate signal and thus has a high potential predictability (e.g., Chen and Van den Dool 1997; Sugi et al. 1997; Nakaegawa et al. 2003).

4. GFS summer low-level circulation

General predictive features of the GFS summer low-level circulation (represented by 850-mb streamfunction, S850) are illustrated in Fig. 1. The climatological S850 (Fig. 1a) shows that the GFS can capture reasonably well the important features of the Asian summer monsoon circulation, including the Pacific subtropical high, the Asian low, and the cross-equatorial high over the IO. These circulation systems contain different predictive features. The climate signal (Fig. 1b) is prominent over the tropical oceans, including the Arabian Sea, the Bay of Bengal, the western and central Pacific, and the Gulf of Mexico. This feature suggests the effective impacts of tropical SSTA on the potential predictability of the summer tropical circulation in the GFS hindcasts. On the other hand, the climate noise (Fig. 1c) is striking in the extratropics, but relatively indiscernible in the tropics. Its maximum centers spatially concur with the extratropical storm tracks, indicating the important contribution of transient eddies or high-frequency natural variability to the unpredictable climate noise (e.g., Madden 1976; Blackmon et al. 1984). The signal-to-noise ratio (Fig. 1d) reveals that the potential predictability is strong over the tropics and weak over the extratropics. In the tropics, the predictability is much larger over the western-central Pacific than the IO. The most significant interannual variability in the Pacific is the El Niño-Southern Oscillation (ENSO), which prompts strong air-sea coupling to cause a high predictability in the overlying circulation (e.g., Chen and Van den Dool 1997; Shukla et al. 2000). For the circulation over the Indian monsoon region, the contribution of ENSO to its interannual variability is comparable to those regional-scale fluctuations arising from an internal oscillation unrelated to SST forcing (Goswami 1998). The lack of dominant SST influence leads to a low predictability for the Indian monsoon circulation.

To comply with the above predictive features, the tropical low-level circulation in the Indo-Pacific region is separated into three sections for analysis: the eastern Pacific Niño (EPN; 160°E–80°W, 30°S–30°N) region, the western Pacific monsoon (WPM; 100°E–160°E, 30°S–30°N) region, and the Indian Ocean monsoon (IOM; 40°E–100°E, 30°S–30°N) region (see Fig. 1d). These three circulations are related to the ENSO, the western Pacific-East Asian monsoon, and the Indian monsoon, respectively.

5. Predictability of GFS summer low-level tropical circulation

For the circulations over the EPN, WPM, and IOM regions, their 1979–2003 PPC time series are shown in Fig. 2. They are the mean of all 45 PPC values obtained in each summer. The long-term mean is 0.59 in both the EPN and WPM regions and 0.40 in the IOM region. The reproducibility or potential predictability of the GFS tropical low-level circulation anomalies tends to be higher over the Pacific than over the IO. This result is in agreement with that of the signal-to-noise ratio analysis and other AGCM predictions (e.g., Kang et al. 2004).

The above PPC time series have a simultaneous correlation coefficient of 0.69 between the EPN and WPM regions, 0.31 between the IOM and EPN regions, and 0.41 between the IOM and WPM regions. The WPM circulation tends to vary coherently with the predictability of the EPN circulation, rather than the IOM circulation. This feature suggests that consideration of predictability characteristics of the WPM and IOM circulations as an entity is not applicable to all models.

For each of the three tropical circulations, its potential predictability in each summer is categorized as the high (denoted by "+")/low (denoted by "−") state when the corresponding PPC value is larger/smaller than the long-term mean. Table 1 presents a summary of the phase relationship in predictability state for these tropical circulations. For the entire 25 summers, the EPN and WPM circulations have the same predictability state in 21 summers (high in 11 summers and low in 10 summers) and a different state in only four summers. On the other hand, the phase relationship between the IOM circulation and the EPN or WPM circulation seems to be irregular. The IOM circulation is likely affected by a mechanism that is independent of that affecting the EPN and WPM circulations, while the two circulations over the Pacific may be commonly regulated by the same mechanism.

The most likely regulating mechanism in the Pacific is the ENSO. The ENSO phase is inferred from the summer Niño 3.4 (120°–170°W, 6°S–6°N) SSTA, and categorized as the warm (W), cold (C), or normal (N) phase when this SSTA is $\geqq 0.5$°C, $\leqq -0.5$°C, or in between -0.5°C and 0.5°C, respectively. This partition includes nine ENSO (five warm and four cold) cases. As summarized in Table 1, the EPN (WPM) circulation has a high predictability state in five (four) out of the five warm cases, and three (three) out of the four cold cases. The IOM circulation has only two high predictability states in both the warm and cold cases. To consider all the cases together, both the EPN and WPM circulations have a high predictability state in seven out of nine ENSO summers. The corresponding number decreases into four between the IOM and the EPN or WPM circulations, less than a half of the total ENSO cases. The appearance of strong Niño 3.4 SSTA effectively increases the potential predictability of the GFS summer tropical circulation over the Pacific. This result agrees with Shukla et al.'s (2000) finding that the

Table 1. The phase relationship in predictability state among the GFS circulations over the eastern Pacific Niño (EPN) region, the western Pacific monsoon (WPM) region, and the Indian Ocean monsoon (IOM) region for the entire 25 (1979–2003) summers and the nine ENSO summers with warm or cold conditions. The high and low predictability state is denoted as "+" and "−", respectively.

All 25 summers					
		WPM		IOM	
		+	−	+	−
EPN	+	11	2	7	6
	−	2	10	4	8
WPM	+			8	5
	−			3	9
9 ENSO summers					
		WARM		COLD	
		+	−	+	−
EPN		5	0	3	1
WPM		4	1	3	1
IOM		2	3	2	2
		WPM		IOM	
		+	−	+	−
EPN	+	7	1	4	4
	−	0	1	0	1
WPM	+			4	3
	−			0	2

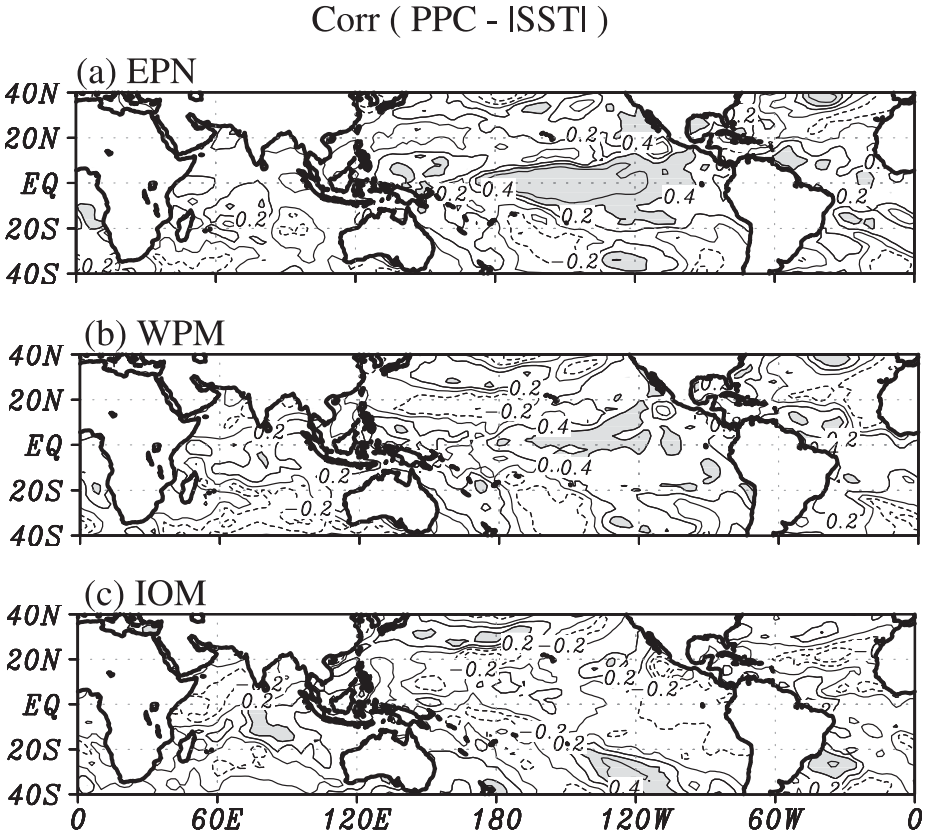

Fig. 3. The simultaneous correlation patterns of the intensity of SST anomalies (|SST|) to the PPC value in the (a) EPN, (b) WPM, and (c) IOM regions. The shading indicates areas where the correlation is significant at the 95% level. The contour intervals are 0.2.

intensity of the SSTA is an important factor affecting the predictability of model circulation.

The relationship between the potential predictability and the SST intensity (absolute value of SST anomaly, denoted as |SST|) is examined in terms of correlation patterns between the SST intensity and the PPC time series of the tropical circulation (Fig. 3). Correlation coefficients significant at the 95% level are shaded. The significant patterns indicate that the potential predictability of the EPN and WPM circulations are mainly connected with |SST| in the tropical eastern Pacific, but only partially related to |SST| in the tropical western Pacific and the IO (Figs. 3a–b). The potential predictability of the IOM circulation primarily links to |SST| in the tropical central IO (Fig. 3c), rather than in the tropical Pacific. The predictability of the EPN and WPM circulations tends to be jointly regulated by the intensity of the tropical eastern-Pacific SSTA, while the predictability of the IOM circulation is mainly affected by the SST intensity in the tropical central IO. Note that the SSTA over the WPM and IOM regions is generally smaller than that over the EPN region. However, the large absolute SST value in the former regions could generate a large diabatic heating anomaly to compete with that in the latter region. Detailed response processes of the atmosphere to SST anomalies need to be further examined.

6. Predictability source for the EPN and WPM circulations

This section investigates the source of predictability provided by the SSTA for the GFS summer tropical low-level circulations over the Pacific. Since the EPN and WPM circulations tend to have a coherent PPC variability, all summers in which these two circulations have the same predictability state are divided into four predictability types for analysis. There are 11 summers with the high pre-

dictability state (see Table 1). They are partitioned, in accordance with the phase of the Niño 3.4 SSTA, into warm, cold, and normal phases, which are denoted as the PPC(+)W, PPC(+)C, and PPC(+)N types, respectively. Nine out of ten summers with the low predictability state occur in the normal SST phase. These nine summers are grouped together as the PPC(−)N type. For these four predictability types, their member years, anomalous Niño 3.4 SST states, and PPC values for the EPN and WPM circulations are displayed in Table 2.

The composite anomalies of PPC(+)W and PPC(+)C types are mainly opposite in the spatial patterns. To avoid redundancy, their composite difference anomalies (warm minus cold) are analyzed in Fig. 4, including SST, 850-mb velocity potential (X850), S850, and tropical Walker circulation and 500-mb vertical motion (ω500) along the Equator. The Walker circulation is expressed by a mass flux function $\psi_m = \int_p^{p_0} u_d \, dp$ (Newell et al. 1974), where u_d is the zonal divergent wind and the vertical integral is from a given pressure level to $p_0 = 1000$ mb. Hereafter, all anomalies significant at the 95% level are shaded. As revealed by the significant pattern, the SST difference anomalies (Fig. 4a) exhibit an El Niño-like structure, an elongated and strong warming over the tropical eastern Pacific and a minor cooling over the tropical western Pacific and the Maritime Continent. The SSTA in the IOM region is generally insignificant. The east-west SST contrast in the Pacific forces a pair of tropical X850 anomalies (Fig. 4b), consisting of a convergent (positive) center over the eastern Pacific and a divergent (negative) center over the western Pacific. In correspondence to this X850 anomaly pair, S850 anomalies (Fig. 4c) exhibit a Rossby-wave-like pattern, featuring a pair of equatorial symmetric anomalous lows straddling the Equator over the western and central Pacific. This pattern spatially covers the regions of the EPN and WPM circulations and thus accounts for their coherent predictability. The corresponding ψ_m anomaly is a significant cell across the Pacific (Fig. 4d). As indicated by the ω500 anomaly (Fig. 4e), this cell has an ascending center in the EPN region (~170°W) and a descending center in the WPM region (~130°E). This ψ_m cell acts as an atmospheric bridge to convey the impacts of ENSO SSTA onto the EPN and WPM circulations simultaneously, leading to a coherent predictability state for these two circulations.

For the normal SST cases, the composite anomalies for the PPC(+)N and PPC(−)N types are compared in Fig. 5. Their significant SST anomalies (Figs. 5a–b) appear as an elongated negative anomaly over the tropical eastern Pacific. The X850 anomalies (Figs. 5c–d) form a significant divergent

Table 2. The four major predictability types of the GFS summer tropical circulation over the Pacific and their associated member years, anomaly state of the Niño 3.4 SST, and the PPC values for circulations in the EPN and WPM regions.

Type	Year	Niño 3.4 SST anomaly	PPC	
			EPN	WPM
PPC(+)W	1982	warm	0.85	0.75
	1991		0.83	0.77
	1997		0.86	0.83
	2002		0.62	0.78
	AVG		0.79	0.78
PPC(+)C	1988	cold	0.9	0.92
	1998		0.73	0.79
	1999		0.82	0.85
	AVG		0.82	0.85
PPC(+)N	1986	normal	0.65	0.72
	1992		0.68	0.65
	1984		0.73	0.67
	2000		0.74	0.86
	AVG		0.70	0.73
PPC(−)N	1980	normal	0.18	0.2
	1990		0.09	0.53
	1993		0.38	0.37
	1994		0.49	0.55
	2001		0.27	0.25
	2003		0.4	0.37
	1981		0.52	0.51
	1989		0.56	0.57
	1995		0.24	0.22
	AVG		0.35	0.40
1979–2003 mean			0.59	0.59

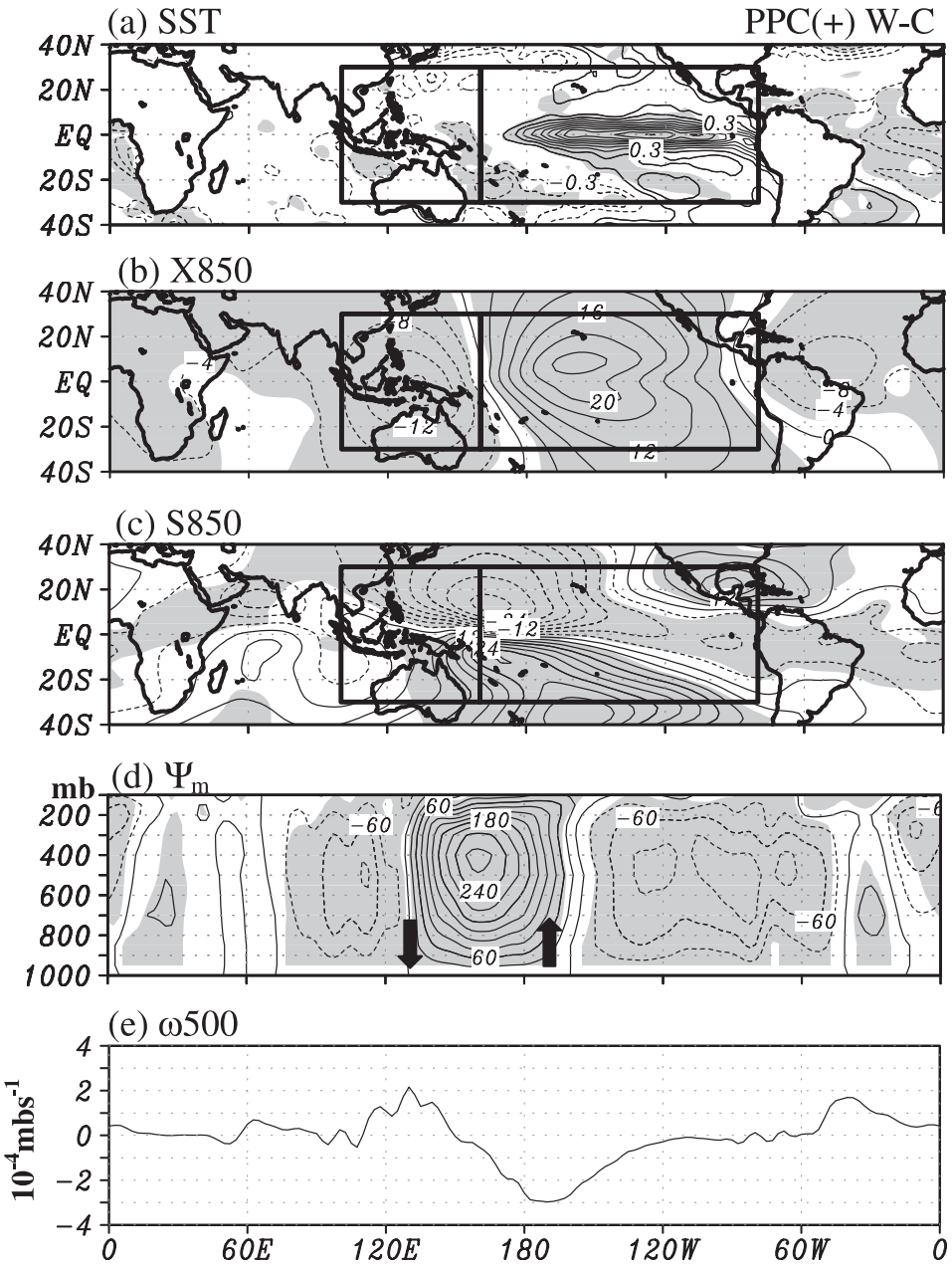

Fig. 4. Composite difference anomalies of (a) SST, (b) 850-mb velocity potential, (c) 850-mb streamfunction, and (d) vertically-integrated mass flux function and (e) 500-mb vertical motion at the Equator between the PPC(+)W and PPC(+)C types (W minus C) of the EPN and WPM circulations. The contour intervals are 0.3°C in (a), 4×10^5 m^2 s^{-1} in (b) and (c), and 30 m s^{-1} mb in (d). In (a), zero contour is suppressed. Anomalies significant at the 95% level are shaded.

center over the tropical eastern Pacific and a complementary convergent center over the tropical western Pacific. For S850 anomalies, a pair of equatorial symmetric anomalous highs situates across the EPN and WPM regions (Figs. 5e–f), as a Rossby-wave response. All the SST, X850, and S850 anomalies exhibit similar patterns between the PPC(+)N and PPC(−)N types, with a stronger intensity in the former than the latter. Their spatial patterns highly resemble those of the strong SST

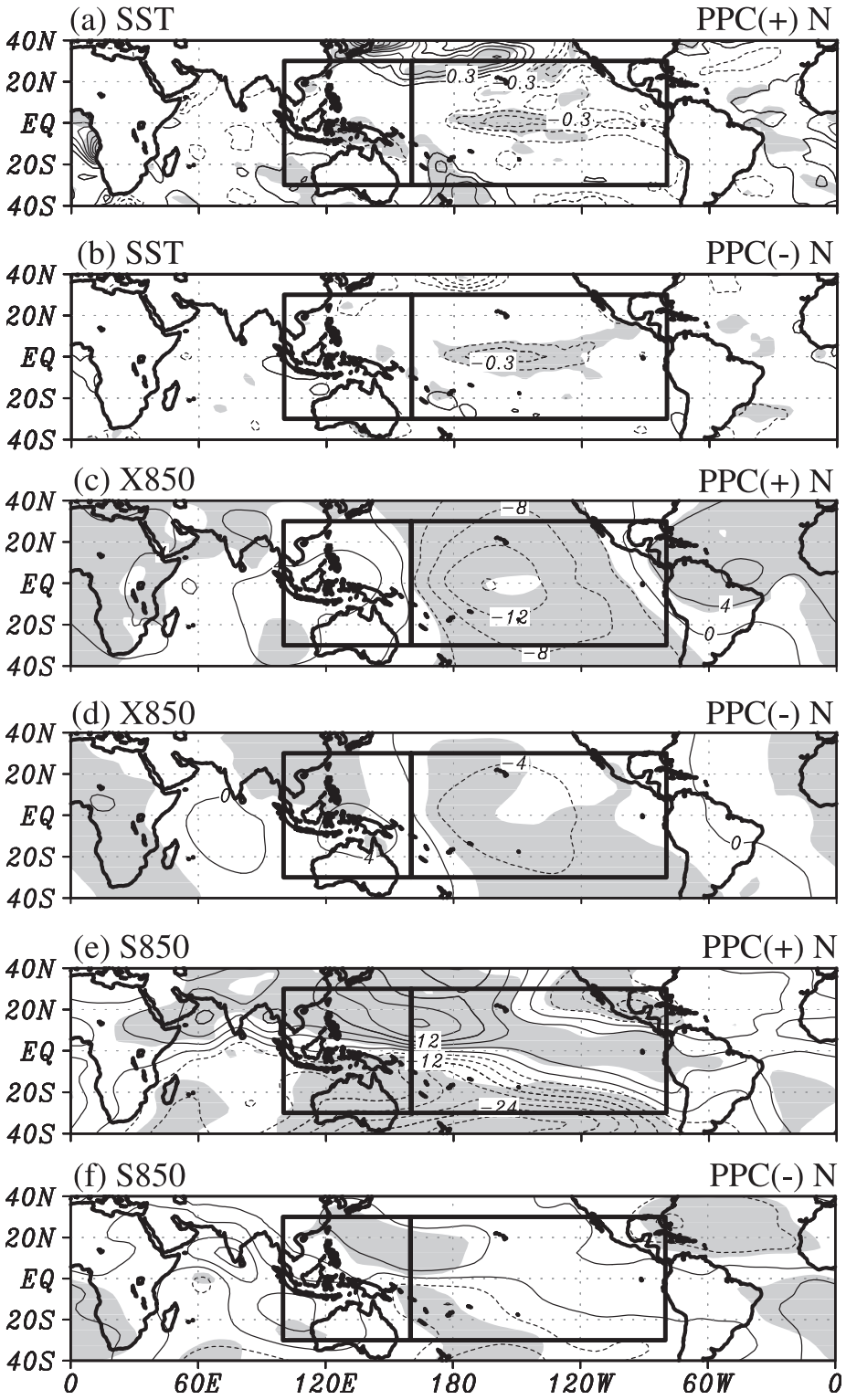

Fig. 5. As in Fig. 4, except for composite anomalies for the PPC(+)N and PPC(−)N predictability types. In (a), the contour intervals are 0.15°C.

conditions in Fig. 4, except with corresponding reversed signs.

The above analyses demonstrate that the tropical eastern Pacific SSTA appears as the major predictability source for both the EPN and WPM circulations in the GFS hindcast. Stronger SST anomalies tend to induce stronger predictability. The associated regulating mechanisms include the processes of Rossby-wave response and tropical Walker circulation variability.

7. Predictability source for the IOM circulation

The predictability states of the IOM circulation are categorized into four major types in Table 3. This categorization employs two criteria: the PPC value of the IOM circulation and SST value averaged over the tropical central IO (70°–90°E, 0°–14°S) where SST intensity is significantly correlated with the PPC value (see Fig. 3c). A summer with a PPC value larger (smaller) than its long-term mean is defined as the high (low) predictability state. The area-averaged SST value has a long-term mean of 27.7°C and a standard deviation (SD) of 0.20°C. A summer with an anomalous SST value larger/smaller than 0.16°C/−0.16°C (0.8 SD) is categorized as the anomalous warm/cold condition, while a value between 0.16°C and −0.16°C is the normal condition. The high predictability state has five/three/three summers concurrent with an anomalous warm/cold/normal condition in the tropical central IO. The low predictability state is mainly coexistent with the normal SST condition as signified by 12 summers in the PPC(−)N type. The IOM predictability in the GFS hindcast tends to increase when forced by strong SST anomalies in the tropical central IO.

The composite difference anomalies between the PPC(+)W and PPC(+)C types (warm minus cold) of the IOM circulation are displayed in Fig. 6. Significant SST anomalies exhibit major tropical warming centers in the IO and the eastern Pacific (Fig. 6a). These warm SST anomalies cause two anomalous convergent centers in the overlying X850 anomalies. Meanwhile, two complementary divergent anomalies occur in the Atlantic Ocean and the Maritime Continent, revealing a global wavenumber-2 structure. To the west of the convergent centers, the Rossby-wave response of tropical rotational circulation results in two meridional pairs of anomalous lows in S850 anomaly (Fig. 6c), a strong and significant one over the IOM region and a moderate one over the western Pacific.

Table 3. As in Table 2, except for the four major predictability types of the IOM circulation.

Type	Year	Indian Ocean SST anomaly	PPC IOM
PPC+(W)	1998	warm	0.60
	1992		0.64
	2002		0.73
	2003		0.53
	1991		0.55
	AVG		0.61
PPC+(C)	1979	cold	0.71
	1989		0.57
	1984		0.43
	AVG		0.57
PPC+(N)	2001	normal	0.52
	1999		0.66
	2000		0.56
	AVG		0.58
PPC−(N)	1997	normal	0.10
	1983		0.29
	1987		0.39
	1995		0.13
	1996		0.29
	1990		0.14
	1981		0.37
	1980		0.11
	1982		0.27
	1993		0.28
	1994		0.30
	1985		0.10
	AVG		0.23
1979–2003 mean			0.42

As indicated by ψ_m and $\omega 500$ anomalies along the Equator (Figs. 6d–e), the strong IOM circulation anomalies directly link with anomalous upward motion associated with the convergent center and warm SSTA over the tropical central IO. This sug-

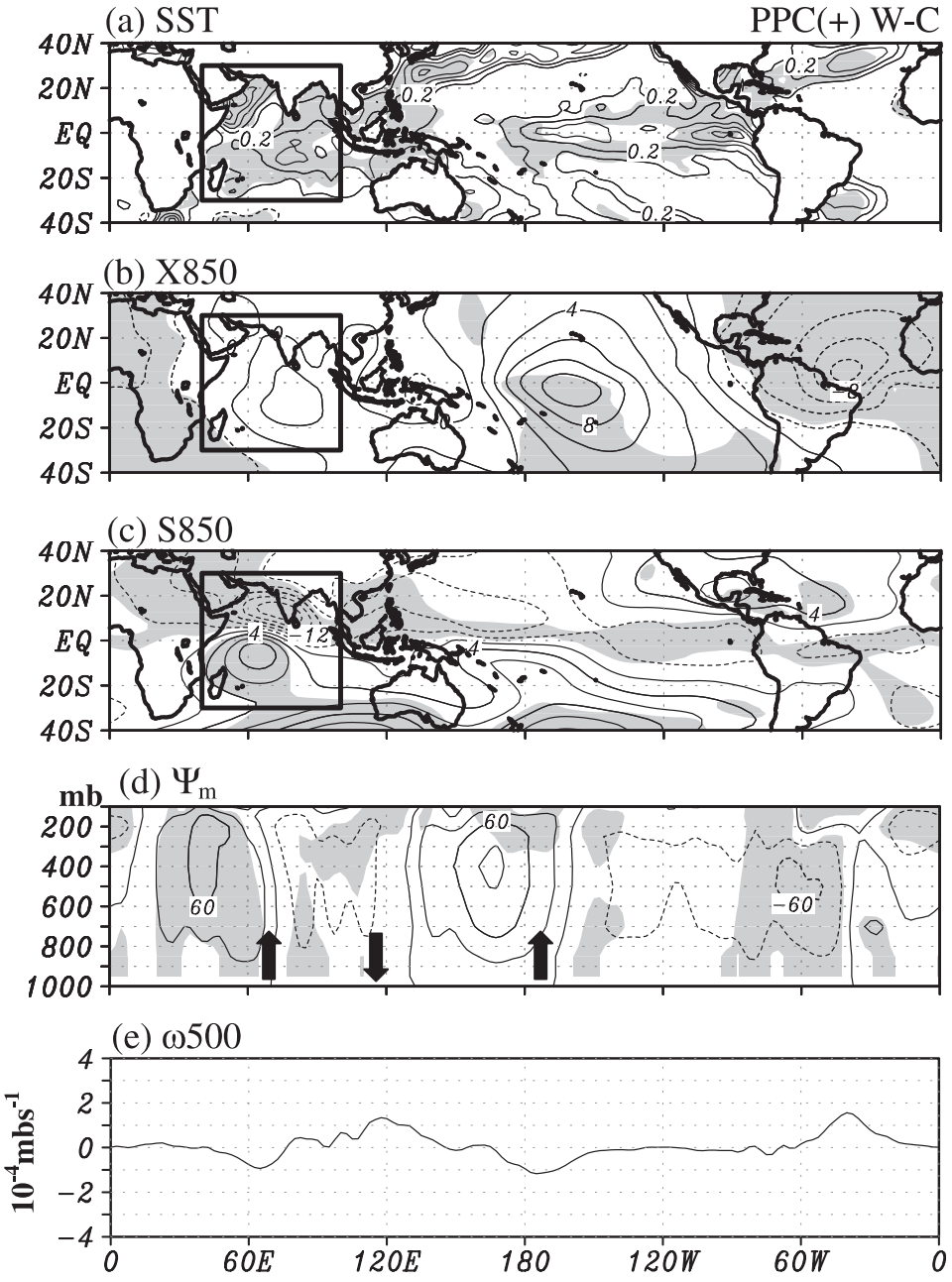

Fig. 6. As in Fig. 4, except for the composite difference anomalies for the IOM circulation. The contour intervals are 0.1°C in (a) and 2×10^5 m^2 s^{-1} in (b).

gests that the strong in situ SSTA in the tropical central IO act as the major predictability source for the IOM circulation in the PPC(+)W and PPC(+)C types.

For the case without a strong SSTA in the central IO, composite anomalies for the PPC(+)N type are shown in Fig. 7. The tropical SST features include strong and significant warm anomalies in the eastern Pacific (Fig. 7a). X850 anomalies (Fig. 7b) respond with a convergent center over the central-eastern Pacific and a divergent center over Africa and the Atlantic, showing a wavenumber-1-like structure. In the IO, there is a moderate-intensity but still significant SST dipole pattern,

with positive anomalies in the east and negative anomalies in the west. This anomalous SST dipole modulates regional X850 anomalies to have a relatively convergent section in the eastern IO and a relatively divergent section in the western IO and Africa. This X850 anomaly pair coincides with a meridional pair of anomalous lows in S850 field across the equatorial IO (Fig. 7c). It also concurs with an ascending center in the eastern IO around 70°E and a descending center in the western IO around 50°E (Fig. 7e), forming a significant local ψ_m cell in the IOM region (Fig. 7d). This ψ_m cell and its associated vertical motion and X850

strength of the meridonal pair of anomalous lows across the IO, leading to an increased predictability for the IOM circulation. These analyses suggest that the predictability source for the IOM circulation in the PPC(+)N type primarily comes from the local SST dipole pattern, rather than the remote SSTA.

The appearance (disappearance) of in-phase SST anomalies in the IO and the tropical eastern Pacific suggests the occurrence (absence) of a Pacific-IO connection, which is particularly significant during the ENSO period (e.g., Kug and Kang 2006; Kug et al. 2006). This connection is mainly via the tropical Walker circulation variability, i.e., the so-called atmospheric bridge (e.g., Wang 1992; Klein et al. 1999; Chen and Lu 2000; Lau and Nath 2000, 2003; Lau and Wang 2006). According to these features, one may examine SST anomalies in Fig. 6a to infer that the PPC(+)W and PPC(+)C types of the IOM circulation tend to concur with a Pacific-IO connection. This connection can go through an atmospheric bridge built by a series of well-organized ψ_m cells across the regions from the eastern Pacific into the IO in Fig. 6d. For the PPC(+)N type in Fig. 7, its SSTA shows a dipole pattern in the IO and are not in phase between the IO and the tropical eastern Pacific. The IO SST dipole is generally considered to result from local air-sea coupled variability that is largely independent of the Pacific SST (e.g., Saji et al. 1999; Webster et al. 1999). The ψ_m pattern in Fig. 7d exhibits a dominant cell in the tropical western Pacific, but does not have well-organized cells in the 80°–120°E and 30°–40°W regions. The atmospheric bridge is incomplete and cannot convey impacts from the eastern Pacific into the IO, suggesting an inappreciable Pacific-IO connection. The above analyses reveal that the IOM circulation may or may not link with the Pacific SST forcing. Therefore, the predictability state of the IOM circulation is not so coherent with that of the WPM and EPN circulations.

8. Model vs. observed predictability

The model characteristics normally differ to some extent from the real atmosphere. It is of interest to compare the model predictability with the observed one. The observed seasonal mean field may be considered to consist of three components: a forced component, an internal source component, and a noise component (e.g., Zwiers 1996; Zheng and Frederiksen 1999). The forced component results from atmospheric response to slowly-varying forcing, such as SST, sea ice, and greenhouse gas (e.g., Manabe et al. 1991; Lau and Nath 1994; Honda et al. 1999), while the internal source component originates from atmospheric variability induced by internal dynamics, land surface processes, and soil moisture (e.g., Zheng and Frederiksen 1999). The noise component mainly attributes to high-frequency weather variability. The forced and internal source components are considered to be potentially predictable on a seasonal timescale, while the noise component is unpredictable (e.g., Lorenz 1973; Madden 1976). The variance of the predictable (unpredictable) components may be considered the signal (noise) of observations. The observed predictability may thus be interpreted from the signal-to-noise ratio computed from the 1979–2003 S850 fields of the National Centers for Environmental Prediction-National Center for Atmospheric Research (NCEP-NCAR) reanalysis data (Kalnay et al. 1996). Readers are referred to Zheng et al. (2000) for the statistical schemes used to estimate these variances.

The signal-to-noise ratios of observations (Fig. 8) and the GFS (Fig. 1d) are consistent, both being

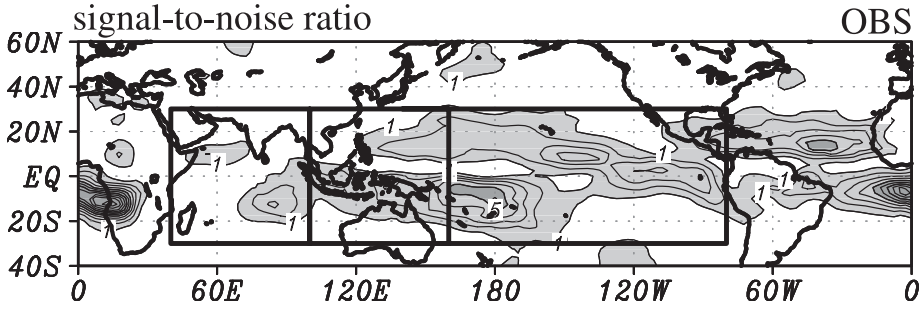

Fig. 8. As in Fig. 1d, except for the observed signal-to-noise ratio of summer S850 computed from the NCEP-NCAR reanalysis data.

high in the tropics and low in the extratropics. However, their regionality differs in many aspects. The GFS has a maximum center in the western-central section of the North Pacific, while observations show a much lower magnitude in that region. In the IO, observations show a regional center in the eastern section, which disappears in the GFS. Additional maximum centers appear in the tropical eastern Pacific, the Atlantic, and western Africa for observations, but not for the GFS. The GFS and observed predictability features differ noticeably in the summer monsoon region, such as the IO and the western Pacific. This difference can be partially explained by the fact that the real SSTA in this region is a response to atmospheric forcing or active air-sea interaction processes, but not an external forcing for atmosphere (e.g., Lau and Nath 2000; Wang et al. 2004; Kang and Shukla 2006). The lack of processes regarding air-sea interactions and atmospheric feedback to oceans in the two-tier system was found to be largely responsible for the AGCM's incapability to faithfully reproduce the observed summer monsoon system (e.g., Kang et al. 2004; Wang et al. 2004, 2005).

9. Concluding remarks

Previous studies have suggested that the low-level circulation anomaly is a potentially useful field for predicting Asian summer monsoon rainfall. The main purpose of this study is to examine the potential predictability of summer (June–August) 850-mb tropical circulation from a 10-member SMIP-type ensemble hindcast conducted for the period 1979–2003 with the Central Weather Bureau (CWB) Global Forecast System (GFS) model. The major tropical circulations are partitioned into three sub-regions for analysis: the eastern Pacific Niño (EPN; 160°E–80°W, 30°S–30°N) region, the western Pacific monsoon (WPM; 100°E–160°E, 30°S–30°N) region, and the Indian Ocean monsoon (IOM; 40°E–100°E, 30°S–30°N) region. The major predictability sources for these circulations and the associated regulating processes are investigated.

Analyses reveal three major predictability features for the GFS summer tropical low-level circulation. First, the potential predictability of the tropical circulation is generally higher over the Pacific than over the IO. Second, the predictability of the WPM circulation tends to vary from year to year in a coherent manner with the EPN circulation, but less coherently with the IOM circulation. This result suggests that the predictability of the WPM and IOM circulations should be examined separately. Third, the major predictability source for the EPN and WPM circulations is tropical SST anomalies in the eastern Pacific, while that for the IOM circulation is local SST anomalies in the IO. Stronger SST anomalies normally give rise to a higher predictability.

The dynamic processes regulating circulation predictability over the Pacific and the IO are different. Over the Pacific, strong SST anomalies in the tropical eastern Pacific force a pair of low-level divergent-convergent dipole anomalies with one center in the EPN region and the other in the WPM region. This dipole anomaly regulates the EPN and WPM circulations via its associated tropical Walker circulation cell across the eastern and western Pacific and the processes of Rossby-wave response. As such, SST anomalies in the tropical eastern Pacific act as a common predictability source to modulate the EPN and WPM circulations simultaneously, leading to a temporally coherent variation in their predictability. Over the IO, its circulation predictability is modulated in two different ways. The appearance of strong in situ SST anomalies in the tropical central IO directly affects the IOM circulation via the processes of Rossby-wave response. For the situation without strong in situ SST anomalies, a local SST dipole pattern in the IO primarily maintains the predictability of the IOM circulation via the regional Walker circulation cell across the eastern and western IO.

The potential predictability of the GFS summer tropical circulation analyzed in this study simply reflects atmospheric response to the external SST forcing in a two-tier prediction system. This system cannot simulate the processes of air-sea interactions and atmospheric feedback to oceans, while these processes are found to be important in the Asian monsoon system. Such inherent deficiencies make the predictive features of the GFS differ noticeably from observations, particularly in the Asian summer monsoon region. The conclusions of this study need to be used with cautions. They are only applicable to the two-tier AGCM prediction, but not to the coupled ocean-atmosphere model prediction or the real atmosphere. The predictability features of the summer tropical low-level circulation analyzed in this study are new but based on only one AGCM. It is not clear whether such predictability features are common to other AGCMs. To answer this question, future study is needed to analyze

more AGCM experiments compiled by the model-intercomparison project.

Acknowledgements

The authors wish to thank two anonymous reviewers for their valuable comments. This study was jointly supported by the Short-term Climate Prediction Project of the Central Weather Bureau, Taiwan, and National Science Council, Taiwan, under NSC 93-2625-Z-052-001 and NSC 94-2625-Z-052-001. Bin Wang acknowledges the support provided by APEC Climate Center through the Climate Prediction and Application to Society (CliPAS) project.

References

Arakawa, A., and W. H. Schubert, 1974: Interaction of a cumulus cloud ensemble with the large-scale environment, Part I. *J. Atmos. Sci.*, **31**, 674–701.

Bengtsson, L., U. Schlese, E. Roeckner, M. Latif, T. P. Barnett, and N. Graham, 1993: A two-tier approach to climate forecasting. *Science*, **261**, 1026–1029.

Blackmon, M. L., Y. -H. Lee, and J. M. Wallace, 1984: Horizontal structure of 500-mb height fluctuations with long, intermediate, and short time scales. *J. Atmos. Sci.*, **41**, 961–979.

Chen, J. -M., F. -C. Lu, S. -L. Kuo, and C. -F. Shih, 2005: Summer climate variability in Taiwan and associated large-scale processes. *J. Meteor. Soc. Japan*, **83**, 499–516.

Chen, J. -M., and M. -M. Lu, 2000: Interannual variation of the Asian-Pacific atmospheric climate system in association with the summer SST changes. *Terres. Atmos. Ocean*, **11**, 833–860.

Chen, W. Y., and H. M. Van den Dool, 1997: Atmospheric predictability of seasonal, annual, and decadal climate means and the role of ENSO cycle: A model study. *J. Climate*, **10**, 1236–1254.

Detering, H. W., and D. Etling, 1985: Application of the E-e turbulence model to the atmospheric boundary layer. *Bound. -Layer Meteor.*, **33**, 113–133.

Goswami, B. N., 1998: Interannual variations of Indian summer monsoon in a GCM External condition versus internal feedbacks. *J. Climate*, **11**, 501–522.

Harshvardhan, R. Davies, D. Randall, and T. Corsetti, 1987: A fast radiation parameterization for atmospheric circulation models. *J. Geophys. Res.*, **92**, 1009–1016.

Honda, M., K. Yamazaki, H. Nakamura, and K. Takeuchi, 1999: Dynamic and thermaldynamic characteristics of atmospheric response to anomalous sea-ice extent in the Sea of Okhotsk. *J. Climate*, **12**, 3347–3358.

Kalnay, E., and Coauthors, 1996: The NCEP/NCAR 40-year Reanalysis Project. *Bull. Amer. Meteor. Soc.*, **77**, 437–471.

Kanamitsu, M., and Coauthors, 2002: NCEP-DOE AMIP-II Reanalysis (R-2). *Bull. Amer. Meteor. Soc.*, **83**, 1631–1643.

Kang, I. -S., J. -Y. Lee, and C. -K. Park, 2004: Potential predictability of summer mean precipitation in a dynamical seasonal prediction system with systematic error correction. *J. Climate*, **17**, 834–844.

Kang, I. -S., and J. Shukla, 2006: Dynamic seasonal prediction and predictability of the monsoon. *The Asian Monsoon*, B. Wang Ed., Springer/Praxis Publisher, New York, 585–612.

Klein, S. A., B. J. Soden, and N. -C. Lau, 1999: Remote sea surface temperature variations during ENSO: Evidence for a tropical atmospheric bridge. *J. Climate*, **12**, 917–932.

Kug, J. -S., and I. -S. Kang, 2006: Interactive feedback between ENSO and the Indian Ocean. *J. Climate*, **19**, 1784–1801.

Kug, J. -S., T. Li, S. -I. An, I. -S. Kang, J. -J. Luo, S. Masson, and T. Yamagata, 2006: Role of the ENSO-Indian Ocean coupling on ENSO variability in a coupled GCM. *Geophys. Res. Lett.*, **33**, doi:10. 1029/2005GL024916.

Kumar, A., A. G. Barnston, and M. P. Hoerling, 2001: Seasonal predictions, probabilistic verifications, and ensemble size. *J. Climate*, **14**, 1671–1676.

Kumar, A., M. Hoerling, M. Ji, A. Leetmaa, and P. Sardeshmukh, 1996: Assessing a GCM's suitability for making seasonal predictions. *J. Climate*, **9**, 115–129.

Kumar, K. K., M. Hoerling, and B. Rajagopalan, 2005: Advancing Indian monsoon rainfall predictions. *Geophys. Res. Lett.*, **32**, L08704.

Kusunoki, S., and C. Kobayashi, 2003: Skill evaluation of probabilistic forecasts by the Atmospheric Seasonal Predictability Experiments. *J. Meteor. Soc. Japan*, **81**, 85–112.

Kusunoki, S., M. Sugi, A. Kitoh, C. Kobayashi, and K. Takano, 2001: Atmospheric seasonal predictability experiments by the JMA AGCM. *J. Meteor. Soc. Japan*, **79**, 1183–1206.

Lau, K. -M., K. -M. Kim, and S. Yang, 2000: Dynamic and boundary forcing characteristics of regional components of the Asian summer monsoon. *J. Climate*, **13**, 2461–2482.

Lau, N. -C., and M. J. Nath, 1994: A modeling study of the relative roles of the tropical and extratropical ST anomalies in the variability if the global atmosphere-ocean system. *J. Climate*, **7**, 1184–1207.

Lau, N. -C., and M. J. Nath, 2000: Impacts of ENSO on the variability of the Asian-Australian monsoons as simulated in GCM experiments. *J. Climate*, **13**, 4287–4309.

Lau, N. -C., and M. J. Nath, 2003: Atmosphere-ocean

variations in the Indo-Pacific sector during ENSO episodes. *J. Climate*, **16**, 3–20.

Lau, N. -C., and B. Wang, 2006: Interactions between the Asian monsoon and the El Niño/Southern Oscillation. *The Asian Monsoon*, B. Wang Ed., Springer/Praxis Publisher, New York, 479–512.

Liou, C. -S., J. -H. Chen, C. -T. Terng, F. -J. Wang, C. -T. Fong, T. E. Rosmond, H. -C. Kuo, C. -H. Shiao, and M. -D. Cheng, 1997: The second-generation global forecast system at the Central Weather Bureau in Taiwan. *Wea. Forecasting*, **12**, 653–663.

Lorenz, E. N., 1973: On the existence of extended range predictability. *J. Appl. Meteor.*, **12**, 543–546.

Louis, J. F., 1979: A parametric model of vertical eddy fluxes in the atmosphere. *Bound. -Layer Meteor.*, **17**, 187–202.

Madden, R. A., 1976: Estimates of the natural variability of time-averaged sea-level pressure. *Mon. Wea. Rev.*, **104**, 942–952.

Manabe, S., R. J. Stouffer, M. J. Spelman, and K. Bryan, 1991: Transient response of a coupled ocean-atmosphere model to gradual change of atmospheric CO_2. Part I: Annual mean response. *J. Climate*, **4**, 785–818.

Miyakoda, K., G. D. Hembree, R. F. Striker, and I. Shulman, 1972: Cumulative results of extended forecast experiments: I. Model performance for winter cases. *Mon. Wea. Rev.*, **100**, 836–855.

Moothi, S., and M. J. Suarez, 1992: Relaxed Arakawa-Schubert: A parameterization of moist convection for general circulation models. *Mon. Wea. Rev.*, **120**, 978–1002.

Nakaegawa, T., M. Sugi, and K. Matsumaru, 2003: A long-term numerical study of the potential predictability of seasonal mean fields of water variables using MRI/JMA AGCM. *J. Meteor. Soc. Japan*, **81**, 1041–1056.

Newell, R. E., J. W. Kidson, D. J. Vincent, and G. J. Boer, 1974: *The general circulation of the tropical atmosphere*. MIT Press, 370 PP. ISBN 0-26-14029-9.

Palmer, T. N., G. Shutts, and R. Swinbank, 1986: Alleviation of a systematic westerly bias in general circulation and numerical weather prediction models through an orographic gravity wave drag parameterization. *Quart. J. Roy. Meteor. Soc.*, **112**, 1001–1039.

Rowell, D. P., 1998: Assessing potential seasonal predictability with an ensemble of multi-decadal GCM simulations. *J. Climate*, **11**, 109–120.

Saha, S., and H. M. Van den Dool, 1988: A measure of the practical limit of predictability. *Mon. Wea. Rev.*, **116**, 2522–2526.

Saji, H. N., B. N. Goswami, P. N. Vinayachandran, and T. Yamagata, 1999: A dipole mode in the tropical Indian Ocean, *Nature*, **401**, 360–363.

Shukla, J., and Coauthors, 2000: Dynamic seasonal prediction. *Bull. Amer. Meteor. Soc.*, **81**, 2593–2606.

Smith, T. M., and R. W. Reynolds, 2003: Extended reconstruction of global sea surface temperatures Based on COADS data (1854–1997). *J. Climate*, **16**, 1495–1510.

Smith, T. M., and R. W. Reynolds, 2004: Improved extended reconstruction of SST (1854–1997). *J. Climate*, **17**, 12466–2477.

Sperber, K. R., J. M. Slingo, and H. Annamalai, 2000: Predictability and relationship between subseasonal and interannual variability during the Asian summer monsoon. *Quart. J. Roy. Meteor. Soc.*, **126**, 2545–2574.

Sugi, M., R. Kawamura, and N. Sato, 1997: A study of SST-forced variability and potential predictability of seasonal mean fields using the JMA global model. *J. Meteor. Soc. Japan*, **75**, 717–736.

Tiedtke, M., 1984: The sensitivity of the time-scale flow to cumulus convection in the ECMWF model. ECMWF's Workshop on Convection in Large-Scale Numerical Models, ECMWF, Reading, United Kingdom, 297–316. [Available from European Center for Medium-Range Weather Forecasts, Shinfield Park, Reading RG2 9AX, United Kingdom.]

Tribbia, J. J., and D. P. Baumhefner, 1988: Estimates of the predictability of low-frequency variability with a spectral general circulation model. *J. Atmos. Sci.*, **45**, 2306–2317.

Wang, B., 1992: The vertical structure and development of the ENSO anomaly mode during 1979–1989. *J. Atmos. Sci.*, **49**, 698–712.

Wang, B., I. -S. Kang, and J. -Y. Lee, 2004: Ensemble simulations of Asian-Australian variability by 11 AGCMs. *J. Climate*, **17**, 803–818.

Wang, B., R. Wu, and T. Li, 2003: Atmosphere-Warm Ocean interaction and its impact on Asian-Australian Monsoon variation. *J. Climate*, **16**, 1195–1211.

Wang, B., Q. Ding, X. Fu, I. -S. Kang, K. Jin, J. Shukla, and F. Doblas-Reyes, 2005: Fundamental challenge in simulation and prediction of summer monsoon rainfall. *Geophys. Res. Lett.*, **32**, L15711.

Webster, P. J., A. Moore, J. Loschnigg, and M. Leban, 1999: Coupled ocean-atmosphere dynamics in the Indian Ocean during 1997–98. *Nature*, **401**, 356–360.

Wu, R., and B. Kirtman, 2005: Roles of Indian and Pacific Ocean air-sea coupling in tropical atmospheric variability. *Clim. Dyn.*, **25**, 155–170.

Zwiers, F. W., 1996: Interannual variability and predictability in an ensemble of AMIP climate simulations conducted with the CCC GCM2. *Clim. Dyn.*, **12**, 825–847.

Zheng, X., H. Nakamura, and J. A. Renwick, 2000: Potential predictability of seasonal means based on

monthly time series of meteorological variables. *J. Climate*, **13**, 2591–2604.

Zheng, X., and C. S. Frederiksen, 1999: Validating interannual variability in an ensemble of AGCM simulations. *J. Climate*, **12**, 2386–2396.

Zheng, X., M. Sugi, and C. S. Frederiksen, 2004: Interannual variability and predictability in an ensemble of climate simulations with the MRI-JMA AGCM. *J. Meteor. Soc. Japan*, **82**, 1–18.